Hierarchical Finite Element Bases for Triangular and Tetrahedral Elements

S. Adjerid * M. Aiffa † J. E. Flaherty ‡

Abstract

We describe a hierarchical basis for the p-version of the finite element method in two and three dimensions. The corresponding stiffness matrices are shown to have good sparsity properties and better conditioning than those generated from existing hierarchical bases.

1 Introduction

The quality of finite element solutions depends on several factors including the size and shape of the elements, the approximation properties of the space S of the finite element solution, and the smoothness of the true solution. From a computational viewpoint, the choice of a basis is critical to the stability and efficiency of the finite element procedure. Because of their simplicity, the approximating space S usually consists of piecewise polynomial functions relative to a partitioning of the problem domain $\Omega \subset \Re^n$, $n = 1, 2, 3$, into N-elements Ω_j, $j = 1, 2, \ldots, N$. Piecewise polynomial bases are usually constructed by (i) transforming Ω_j to a *standard element* K (Figure 1) by a smooth, one-to-one mapping μ_j and (ii) introducing a basis $\{\hat{\phi}_i\}_{i=1}^{n_p}$ of *shape functions* for a space of polynomials $I\!P_p(K)$ of degree not greater than p on K. The shape functions are typically associated with a mesh entity (*e.g.*, vertex, edge, face, region). The inverse functions $\hat{\phi}_i \circ \mu_j^{-1}$ defined on Ω_j must be "pieced" together so that the global approximation on S has the proper continuity. Second-order problems, for example, require that $S \subset H^1$.

If μ_j is not affine, $\hat{\phi}_i \circ \mu_j^{-1}$ will not necessarily be polynomial. Non-affine mappings are used to represent a curved boundary of the domain Ω for use, for example, with the p-version of the finite element method [2], where improved approximate solutions are obtained by increasing the degree p of $I\!P_p(K)$. In this case, S may not be a subset of the exact-solution space because $\bigcup_{j=1}^{N} \Omega_j \neq \Omega$. Nevertheless, an optimal order of accuracy can be achieved if "regular" mappings of degree p [4] are used to represent elements with curved boundaries [4, 6].

*Department of Mathematics, Virginia polytechnic Institute and State University Blacksburg, VA 24061

†Department of Mathematics, Pennsylvania State University, University Park, PA 16802

‡Scientific Computation Research Center, Rensselaer Polytechnic Institute, Troy, NY 12180

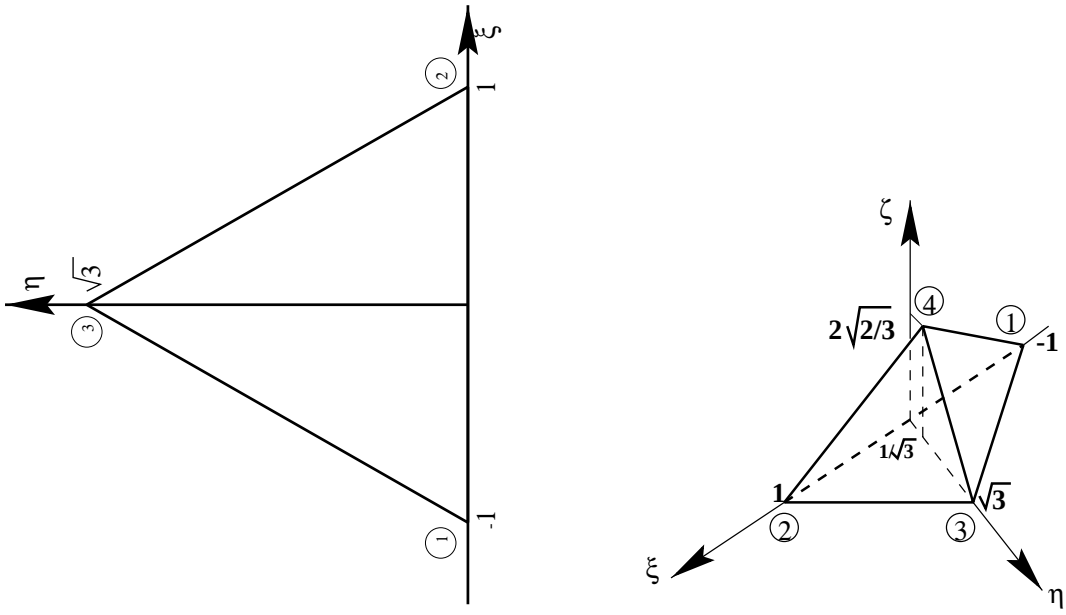

Figure 1: Reference element K in two (left) and three (right) dimensions.

A *hierarchical basis* has the property that the basis of degree $p+1$ is obtained as a correction to the degree p basis. The entire basis need not be reconstructed when the polynomial degree is increased. This property is desirable, if not essential when using the p-version of the finite element method. Shape functions for a one-dimensional hierarchical basis are defined as integrals of Legendre polynomials [10] giving them favorable orthogonality properties that lead to sparse and well conditioned stiffness matrices. Shape functions on square and rectangular-parallelepiped elements may be defined as tensor products of their one-dimensional counterparts to inherit some favorable orthogonality properties [1]. This, however, is not the case with shape functions for triangular and tetrahedral elements [5, 10] where the condition number of the stiffness matrix may increase exponentially with p. To alleviate this, Carnevali *et al.* [3], introduced a new hierarchical basis for triangles and tetrahedra which were constructed so that edge, face, and region shape functions of degree p are orthogonal to those of degree not exceeding $p-2$, $p-3$, and $p-4$, respectively. This basis provided better conditioning than the earlier ones, but condition numbers of stiffness matrices still have an exponential growth with p. Mandel [7, 8] used partial and complete orthogonalizations to construct basis functions on hexahedral elements that were used to furnish preconditioners to multilevel domain decomposition algorithms. These greatly reduced the condition numbers of stiffness matrices for Poisson and linear elasticity problems.

Herein, we introduce new bases for triangles and tetrahedra that have better conditioning than both the Szabó and Babuška [5, 10] and Carnevali *et al.* [3] bases. The construction consists of modifying the Szabó-Babuška basis by orthogonalizing shape functions associated with faces in two dimensions and faces and regions in three dimensions.

2 Hierarchical Shape Functions

2.1 One-Dimensional Shape Functions

The one-dimensional hierarchical basis is defined on the reference "element" $K := \{\xi \mid -1 \le \xi \le 1\}$. For $p \ge 1$, there are two shape functions associated with vertices at $\xi = -1, 1$

$$\hat{\phi}_1^0(\xi) = \frac{1-\xi}{2}, \quad \hat{\phi}_2^0(\xi) = \frac{1+\xi}{2}, \quad \xi \in K, \tag{2.1a}$$

and $p-1$ shape functions associated with the "region" $-1 < \xi < 1$

$$\hat{\phi}_i^1(\xi) = \sqrt{\frac{2i+1}{2}} \int_{-1}^{\xi} P_i(t)dt, \quad \xi \in K, \quad i = 1, 2, \ldots, p-1, \tag{2.1b}$$

where $P_i(\xi)$ is the Legendre polynomial of degree i.

2.2 Two-Dimensional Shape Functions

The hierarchical basis is defined in terms of barycentric coordinates on the reference triangle K of Figure 1

$$L_1 = \frac{1}{2}(1 - \xi - \frac{\eta}{\sqrt{3}}), \quad L_2 = \frac{1}{2}(1 + \xi - \frac{\eta}{\sqrt{3}}), \quad L_3 = \frac{\eta}{\sqrt{3}}. \tag{2.2}$$

We see that L_j has unit value at vertex V_j and vanishes on the edge E_j opposite to V_j. In the sequel, we refer to the Szabó-Babuška [10] basis as the "Szabó basis" and that of Carnevali *et al.* [3] as the "Carnefvali basis."

For $p \ge 1$, the Szabó and Carnevali bases have dimension $n_p = (p+1)(p+2)/2$ and consist of:

- Three vertex shape functions

$$\hat{\phi}_i^0(\xi, \eta) = L_i, \quad i = 1, 2, 3. \tag{2.3a}$$

- $3(p-1)$ edge shape functions on edge E_j, $j = 1, 2, 3$,

$$\hat{\phi}_i^{1,j}(\xi, \eta) = L_{j_1} L_{j_2} \mathcal{E}_i(L_{j_1}, L_{j_2}), \quad i = 1, 2, \ldots, p-1, \quad j_1 = j, \quad j_2 = 1 + j_1 \bmod 3, \tag{2.3b}$$

where

$$\mathcal{E}_i(t_1, t_2) = -\frac{8\sqrt{4i+2}}{i(i+1)} P_i'(t_2 - t_1), \tag{2.3c}$$

for the Szabó basis and

$$\mathcal{E}_i(t_1, t_2) = \sum_{k=0}^{i} \frac{(-1)^k}{k+1} \binom{i}{k} \binom{i+1}{k} t_1^k \, t_2^{i-k} \tag{2.3d}$$

for the Carnevali basis.

- $(p-2)(p-1)/2$ face shape functions

$$\begin{aligned}\hat{\phi}^2_{i_k+r} =& L_1L_2L_3\,\mathcal{F}_{r_1r_2}(L_1,L_2,L_3), \quad i_k=(k-3)(k-2)/2, \\ & r=1,2,\ldots,k-2, \quad r_1+r_2=k-3, \quad k=3,4,\ldots,p,\end{aligned} \tag{2.3e}$$

where

$$\mathcal{F}_{r_1r_2}(t_1,t_2,t_3) = P_{r_1}(t_2-t_1)\,P_{r_2}(2t_3-1). \tag{2.3f}$$

for the Szabó basis and

$$\begin{aligned}\mathcal{F}_{r_1r_2}(t_1,t_2,t_3) = \sum_{i=0}^{r_2}\sum_{j=0}^{r_1}\left(-\frac{1}{2}\right)^{i+j}\binom{r_1}{j}\binom{r_1+1}{j}\binom{r_2}{i}\binom{r_2+1}{i} \\ \times\frac{i!\,j!\,(i+j)!\,t_1^{r_1-j}\,t_2^{r_2-i}}{\prod_{k=1}^{i+j}(k(r_1+r_2+2)-k(k-1)/2)}\end{aligned} \tag{2.3g}$$

for the Carnevali basis.

The edge (2.3b,d) and face (2.3e,g) shape functions, respectively, satisfy [3]

$$\int_K \frac{\partial\hat{\phi}_i^{1,j}}{\partial\xi}\,Q(L_1,L_2)d\xi d\eta = \int_K \frac{\partial\hat{\phi}_i^{1,j}}{\partial\eta}\,Q(L_1,L_2)d\xi d\eta = 0, \quad \text{if} \quad \deg(Q)\le\deg(\hat{\phi}_i^{1,j})-3, \tag{2.4a}$$

$$\int_K \frac{\partial\hat{\phi}_i^{2}}{\partial\xi}\,Q(L_1,L_2)d\xi d\eta = \int_K \frac{\partial\hat{\phi}_i^{2}}{\partial\eta}\,Q(L_1,L_2)d\xi d\eta \;\; = 0, \quad \text{if} \quad \deg(Q)\le\deg(\hat{\phi}_i^{2})-4, \tag{2.4b}$$

where Q is a polynomial.

2.3 Three-Dimensional Shape Functions

The barycentric coordinates on the reference tetrahedron K (Figure 1) expressed in terms of the Cartesian coordinates ξ,η,ζ are

$$\begin{aligned}L_1 &= \frac{1}{2}\left(1-\xi-\frac{\eta}{\sqrt{3}}-\frac{\zeta}{\sqrt{6}}\right), \quad & L_2 &= \frac{1}{2}\left(1+\xi-\frac{\eta}{\sqrt{3}}-\frac{\zeta}{\sqrt{6}}\right), \\ L_3 &= \frac{\eta}{\sqrt{3}}-\frac{\zeta}{2\sqrt{6}}, & L_4 &= \frac{1}{2}\sqrt{\frac{3}{2}}\zeta.\end{aligned} \tag{2.5}$$

Like the two-dimensional case, we see that $L_j=1$ at vertex V_j and vanishes on the face F_j opposite to V_j. Further let E_j be the edge that faces F_4 and F_j, $j=1,2,3$, have in common and let edge E_{j+3} be the edge connecting vertices V_4 and V_j, $j=1,2,3$.

For $p\ge 1$, the Szabó and Carnevali hierarchical bases have dimension $n_p=(p+1)(p+2)(p+3)/6$ and consist of:

- Four vertex shape functions

$$\hat{\phi}_i^0(\xi,\eta,\zeta) = L_i, \quad i = 1,2,3,4. \tag{2.6}$$

- $6(p-1)$ edge shape functions on edge E_j, $j = 1,2,\ldots,6$

$$\hat{\phi}_i^{1,j}(\xi,\eta,\zeta) = L_{j_1}L_{j_2}\mathcal{E}_i(L_{j_1},L_{j_2}), \quad i = 1,2,\ldots,p-1, \tag{2.7a}$$

where

$$j_1 = \begin{cases} 1 + j \bmod 3, & \text{if} \quad 1 \le j \le 3 \\ 1 + j \bmod 4, & \text{if} \quad 4 \le j \le 6 \end{cases}, \tag{2.7b}$$

$$j_2 = \begin{cases} 1 + (j+1) \bmod 3, & \text{if} \quad 1 \le j \le 3 \\ 4, & \text{if} \quad 4 \le j \le 6 \end{cases}. \tag{2.7c}$$

- $4(p-1)(p-2)/2$ face shape functions on face F_j, $j = 1,2,3,4$,

$$\begin{aligned} \hat{\phi}_{i_k+r}^{2,j}(\xi,\eta,\zeta) \; &= L_{j_1}L_{j_2}L_{j_3}\mathcal{F}_{r_1r_2}(L_{j_1},L_{j_2},L_{j_3}), \quad i_k = (k-3)(k-2)/2, \\ &\quad r = 1,2,\ldots,k-2, \quad r_1 + r_2 = k-3, \quad k = 3,4,\ldots,p, \end{aligned} \tag{2.8a}$$

where

$$j_1 = 1 + j \bmod 4, \quad j_2 = 1 + j_1 \bmod 4, \quad j_3 = 1 + j_2 \bmod 4. \tag{2.8b}$$

- $(p-1)(p-2)(p-3)/6$ region shape functions

$$\begin{aligned} \hat{\phi}_{i_k+r}^{3}(\xi,\eta,\zeta) \; &= L_1L_2L_3L_4\,\mathcal{B}_{r_1r_2r_3}(L_1,L_2,L_3,L_4), \quad i_k = (k-4)(k-3)(k-2)/2, \\ &\quad r = 1,2,\ldots,(k-3)(k-2)/2, \quad r_1 + r_2 + r_3 = k-4, \\ &\quad k = 4,5,\ldots,p, \end{aligned} \tag{2.9a}$$

where

$$\mathcal{B}_{r_1r_2r_3}(t_1,t_2,t_3,t_4) = P_{r_1}(t_2 - t_1)\,P_{r_2}(2t_3 - 1)\,P_{r_3}(2t_4 - 1) \tag{2.9b}$$

for the Szabó basis and

$$\mathcal{B}_{r_1r_2r_3}(t_1,t_2,t_3,t_4) = \overline{\mathcal{B}}_{r_100}^{r_1+r_2+r_2}(t_1)\,\overline{\mathcal{B}}_{0r_20}^{r_2+r_3}(t_1,t_2)\overline{\mathcal{B}}_{00r_3}^{r_3}(t_1,t_2,t_3) \tag{2.9c}$$

for the Carnevali basis with

$$\overline{\mathcal{B}}_{r_100}^{(m)}(t_1) = \sum_{i=0}^{r_1}(-1)^i\,i!\binom{r_1}{i}\binom{r_1+1}{i}\frac{(2m+5-i)!}{(2m+5)!}t_1^{r_1-i}, \tag{2.9d}$$

$$\overline{\mathcal{B}}_{0r_20}^{(m)}(t_1,t_2) = \sum_{i=0}^{r_2} i!\binom{r_2}{i}\binom{r_2+1}{i}\frac{(2m+3-i)!}{(2m+3)!}t_2^{r_2-i}(t_1-1)^i, \tag{2.9e}$$

$$\overline{\mathcal{B}}_{00r_3}^{(m)}(t_1,t_2,t_3) = \sum_{i=0}^{r_3} i!\binom{r_3}{i}\binom{r_3+1}{i}\frac{(2m+1-i)!}{(2m+1)!}t_3^{r_3-i}(t_2+t_1-1)^i. \tag{2.9f}$$

The edge (2.7a,2.3d), face (2.8a,2.3g), and region (2.9a,c-f) shape functions, respectively, satisfy [3]

$$\int_K \frac{\partial \hat{\phi}_i^{1,j}}{\partial \xi} Q(L_1, L_2, L_3) d\xi d\eta d\zeta = 0, \quad \text{if} \quad \deg(Q) \leq \deg(\hat{\phi}_i^{1,j}) - 3, \tag{2.10a}$$

$$\int_K \frac{\partial \hat{\phi}_i^{2,j}}{\partial \xi} Q(L_1, L_2, L_3) d\xi d\eta d\zeta = 0, \quad \text{if} \quad \deg(Q) \leq \deg(\hat{\phi}_i^{2,j}) - 4, \tag{2.10b}$$

$$\int_K \frac{\partial \hat{\phi}_i^{3}}{\partial \xi} Q(L_1, L_2, L_3) d\xi d\eta d\zeta = 0, \quad \text{if} \quad \deg(Q) \leq \deg(\hat{\phi}_i^{3,j}) - 5, \tag{2.10c}$$

with similar relations involving $\partial/\partial\eta$ and $\partial/\partial\zeta$.

3 Conditioning of the Hierarchical Basis

In order to illustrate the effect of the basis on the conditioning of the stiffness matrix, consider the bilinear form associated with the Laplacian

$$B(\phi, \psi) = \int_K \nabla\phi \cdot \nabla\psi \, d\omega \tag{3.1}$$

where ∇ is the gradient operator with respect to ξ, η, and, in three dimensions, ζ and $d\omega$ is a surface element in two dimensions and a volume element in three dimensions. Let $\mathbf{\Psi}_p^s = \left\{\hat{\psi}_i^s\right\}_{1 \leq i \leq n_p}$ and $\mathbf{\Psi}_p^c = \left\{\hat{\psi}_i^c\right\}_{1 \leq i \leq n_p}$, respectively, be the Szabó and Carnevali hierarchical bases (§2) of degree p on the reference element K (Figure 1). Assume that the elements of $\mathbf{\Psi}_p^s$ and $\mathbf{\Psi}_p^c$ are ordered with their vertex shape functions first, their edge shape functions second, their face shape functions third, and, in three dimensions, their element shape functions last.

The local stiffness matrices for the Laplacian operator are

$$M_p^t = \left(B(\hat{\psi}_i^t, \hat{\psi}_j^t)\right)_{1 \leq i,j \leq n_p}, \quad t = s, c, \tag{3.2}$$

Further suppose that the shape functions have been rescaled so that M_p^s and M_p^c have unit diagonal entries. Since B is symmetric and non-negative, the eigenvalues $\lambda_1^t \leq \lambda_2^t \leq \cdots \leq \lambda_{n_p}^t$ of M_p^t, $t = s, c$ are real and non-negative. We may readily verify that $\lambda_1^t = 0$ and $\lambda_2^t > 0$. As such, we take the condition number of M_p^t as [1]

$$\kappa(M_p^t) = \frac{\lambda_{n_p}^t}{\lambda_2^t}, \quad t = s, c, \tag{3.3}$$

and show the growth of $\kappa(M_p^s)$ and $\kappa(M_p^c)$ with p for $p = 1, 2, \ldots, 14$ in Figure 2.

Even though the condition number of M_p^c grows more slowly with p than that of M_p^s, the rate is exponential for both bases. In order to gain insight into the problem, we partition the basis into subsets with $\mathcal{V}$, $\mathcal{E}$, $\mathcal{F}$, and $\mathcal{R}$ denoting sets of vertex, edge, face, and region shape functions, respectively. We compute condition numbers of various principal submatrices of the stiffness matrix corresponding to different combinations of

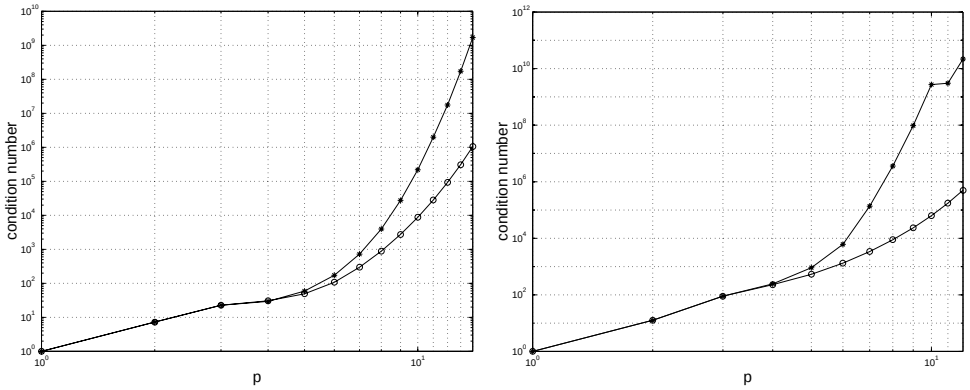

Figure 2: Condition numbers of M_p^s ($*$) and M_p^c ($\circ$) vs. p in two (left) and three (right) dimensions.

Matrix		p							
$\mathcal{V} \cup \mathcal{E}$	M_p^s	1.02e1	1.19e1	1.23e1	1.33e1	1.36e1	1.46e1	1.49e1	1.60e1
	M_p^c	1.01e1	1.01e1	1.01e1	1.01e1	1.01e1	1.01e1	1.01e1	1.01e1
$\mathcal{V} \cup \mathcal{F}$	M_p^s	3.73	1.51e1	6.46e1	3.72e2	2.68e3	2.18e4	1.76e5	1.68e6
	M_p^c	3.00	9.53	3.12e1	1.04e2	3.50e2	1.19e3	4.12e3	1.43e4
$\mathcal{E}$	M_p^s	6.19	6.31	7.09	7.24	8.04	8.24	9.34	9.49
	M_p^c	4.75	4.75	4.75	4.75	4.75	4.75	4.75	4.75
$\mathcal{E} \cup \mathcal{F}$	M_p^s	2.23e1	5.43e1	1.50e2	7.04e2	3.87e3	2.72e4	2.17e5	1.98e6
	M_p^c	2.45e1	4.68e1	9.43e1	2.65e2	8.06e2	2.55e3	8.20e3	2.68e4
$\mathcal{F}$	M_p^s	3.73	1.51e1	6.46e1	3.72e2	2.68e3	2.18e4	1.76e5	1.68e6
	M_p^c	3.00	9.53	3.12e1	1.04e2	3.50e2	1.19e3	4.12e3	1.43e4
$\mathcal{V} \cup \mathcal{E} \cup \mathcal{F}$	M_p^s	2.95e1	5.93e1	1.73e2	7.22e2	3.96e3	2.75e4	2.18e5	1.99e6
	M_p^c	3.06e1	4.92e1	1.07e2	2.97e2	8.86e2	2.75e3	8.72e3	2.82e4

Table 1: Condition numbers of various submatrices of M_p^s and M_p^c in two dimensions.

Matrix Portions	Matrix	p							
		5	6	7	8	9	10	11	12
$\mathcal{V} \cup \mathcal{E}$	M_p^s	3.84e1	4.25e1	4.72e1	5.00e1	5.52e1	5.90e1	6.70e1	7.23e1
	M_p^c	2.55e1	2.55e1	2.55e1	2.55e1	2.55e1	2.55e1	2.55e1	2.55e1
$\mathcal{V} \cup \mathcal{F}$	M_p^s	7.94e1	5.75e2	5.86e3	5.93e4	6.76e5	7.94e6	8.59e6	2.81e7
	M_p^c	1.84e1	4.88e1	1.48e2	4.62e2	1.44e3	4.58e3	1.47e4	4.78e4
$\mathcal{V} \cup \mathcal{R}$	M_p^s	3.00e1	8.57e2	2.53e4	7.64e5	2.27e7	7.00e8	2.19e10	7.06e11
	M_p^c	3.81	8.27	1.89e1	3.97e1	7.70e1	1.43e2	2.49e2	4.18e2
$\mathcal{E}$	M_p^s	1.65e1	2.07e1	2.20e1	2.81e1	2.92e1	4.13e1	4.15e1	5.99e1
	M_p^c	8.22	8.22	8.22	8.22	8.22	8.22	8.22	8.22
$\mathcal{E} \cup \mathcal{F}$	M_p^s	6.40e2	1.61e3	1.37e4	9.46e4	1.04e6	1.08e7	1.12e7	1.76e7
	M_p^c	3.13e2	5.29e2	8.45e2	1.15e3	2.33e3	6.79e3	2.04e4	6.26e4
$\mathcal{E} \cup \mathcal{R}$	M_p^s	4.91e1	1.22e3	2.99e4	8.67e5	2.47e7	7.51e8	1.29e10	1.61e11
	M_p^c	2.45e1	3.74e1	5.29e1	9.60e1	1.84e2	3.50e2	6.30e2	1.08e3
$\mathcal{F}$	M_p^s	6.57e1	5.49e2	5.73e3	5.91e4	6.74e5	7.93e6	8.59e6	2.77e7
	M_p^c	1.54e1	4.87e1	1.47e2	4.62e2	1.44e3	4.58e3	1.47e4	4.78e4
$\mathcal{F} \cup \mathcal{R}$	M_p^s	1.80e2	4.41e3	1.03e5	2.88e6	7.81e7	2.30e9	2.66e9	7.08e9
	M_p^c	4.14e1	1.24e2	3.04e2	9.42e2	3.11e3	1.06e4	3.62e4	1.25e5
$\mathcal{R}$	M_p^s	3.00e1	8.57e2	2.53e4	7.64e5	2.27e7	7.00e8	2.19e10	7.06e11
	M_p^c	3.81	8.27	1.89e1	3.97e1	7.70e1	1.43e2	2.49e2	4.18e2
$\mathcal{V} \cup \mathcal{E} \cup \mathcal{F}$	M_p^s	7.99e2	2.66e3	1.58e4	1.09e5	1.06e6	1.13e7	1.13e7	1.78e7
	M_p^c	3.99e2	6.54e2	1.05e3	1.49e3	2.70e3	7.11e3	2.08e4	6.35e4
$\mathcal{V} \cup \mathcal{E} \cup \mathcal{R}$	M_p^s	7.29e1	1.23e3	3.11e4	8.67e5	2.49e7	7.52e8	1.29e10	1.62e11
	M_p^c	3.66e1	4.46e1	6.80e1	1.17e2	2.14e2	3.93e2	6.93e2	1.17e3
$\mathcal{V} \cup \mathcal{F} \cup \mathcal{R}$	M_p^s	2.12e2	4.43e3	1.11e5	2.88e6	8.18e7	2.30e9	2.67e9	7.14e9
	M_p^c	4.80e1	1.26e2	3.08e2	9.43e2	3.11e3	1.06e4	3.62e4	1.25e5
$\mathcal{E} \cup \mathcal{F} \cup \mathcal{R}$	M_p^s	8.67e2	5.97e3	1.35e5	3.53e6	9.54e7	2.70e9	3.03e9	9.21e9
	M_p^c	5.26e2	1.23e3	2.75e3	6.34e3	1.57e4	4.23e4	1.21e5	3.59e5
$\mathcal{V} \cup \mathcal{E} \cup \mathcal{F} \cup \mathcal{R}$	M_p^s	9.08e2	6.10e3	1.37e5	3.59e6	9.62e7	2.73e9	3.04e9	2.18e10
	M_p^c	5.34e2	1.32e3	3.39e3	8.86e3	2.34e4	6.32e4	1.76e5	5.03e5

Table 2: Condition numbers of various submatrices of M_p^s and M_p^c in three dimensions.

these sets of shape functions and present results in Tables 1 and 2 for two- and three-dimensional problems, respectively. Examining Table 1, we see that the growth of the condition number with p is slow except for those submatrices involving face shape function. Results in Table 2 show a rapid growth of the condition number for submatrices that involve face or region shape functions. Therefore, the cause of the ill conditioning is the interaction of the face and region shape functions with themselves and each other.

4 A New hierarchical Basis

In order to reduce the condition number of the stiffness matrix, we reduce the coupling between the face and region shape functions through orthogonalization. Thus, the new basis $\mathbf{\Psi}_p^n = \left\{\hat{\psi}_i^n\right\}_{1\le i\le n_p}$ has the vertex and edge shape functions of the Szabó basis $\mathbf{\Psi}_p^s$, but the face and, in three dimensions, the region shape functions will satisfy orthogonality conditions. The construction is developed in §4.1 in two dimensions and in §4.2 in three dimensions.

4.1 Two-Dimensional Shape Functions

The two-dimensional basis is constructed to have orthogonal face modes with the Laplacian operator; thus,

$$B(\hat{\psi}_i^n, \hat{\psi}_j^n) = \delta_{ij}, \quad 3p < i, j \le n_p. \tag{4.1}$$

Orthogonal face shape functions $\left\{\hat{\phi}_i^2 := \hat{\psi}_{3p+i}^n\right\}_{1\le i\le n_F}$, $n_F = (p-1)(p-2)/2$ are constructed from the Szabó face shape functions (2.3e,f) using the Gram-Schmidt process, which is expressed by the pseudocode shown in Figure 3.

$k = 1$; $\quad \alpha_1^1 = 1$; $\quad b_1 = B(\hat{\varphi}_1^2, \hat{\varphi}_1^2)$; $\quad \hat{\phi}_1^2 = \alpha_1^1 \hat{\phi}_1^2$;
while ($k \le n_F$) **{**
  for ($l = 1, l < k, ++l$)**{**
    $\beta_l = -\left(\sum_{j=1}^{l} \alpha_j^l B(\hat{\phi}_k^2, \hat{\phi}_j^2)\right)/b_l$;
  }
  for ($j = 1, j < k, ++j$)**{**
    $\alpha_j^k = \sum_{l=j}^{k-1} \beta_l \alpha_j^l$;
  }
  $\alpha_k^k = 1$;
  $b_k = \sum_{j=1}^{k} \alpha_j^k \sum_{i=1}^{k} \alpha_i^k B(\hat{\phi}_i^2, \hat{\phi}_j^2)$;
  $\hat{\phi}_k^2 = \sum_{j=1}^{k} \alpha_j^k \hat{\phi}_j^2$;
}

Figure 3: Pseudocode of the Gram-Schmidt process to generate the orthogonal face shape functions $\hat{\phi}_k^2$, $k = 1, 2, \ldots, n_F$.

The orthogonalization process of Figure 3 involves the evaluation of integrals such as

$$\int_K \left[\frac{\partial \hat{\phi}_i^2}{\partial \xi} \frac{\partial \hat{\phi}_j^2}{\partial \xi} + \frac{\partial \hat{\phi}_i^2}{\partial \eta} \frac{\partial \hat{\phi}_j^2}{\partial \eta} \right] d\xi d\eta, \tag{4.2}$$

which are difficult by either analytical or numerical means for high values of p. Thus, instead of (2.3e,f), we found it easier to replace (2.3f) by

$$\mathcal{F}_{r_1 r_2}(t_1, t_2, t_3) = (t_2 - t_1)^{r_1} \, (2t_3 - 1)^{r_2}. \tag{4.3}$$

Even though the two sets of face shape functions (2.3e,f) and (2.3e, 4.3) differ, the resulting set of orthogonal (normalized) face shape functions can readily be shown to be identical. The integrals (4.2) using (2.3e, 4.3) can be evaluated explicitly as indicated in the following lemma.

Lemma 1. *Let α_i, $i = 1, 2, \ldots, 6$, be non-negative integers and*

$$f = L_1^{\alpha_1} \, L_2^{\alpha_2} \, L_3^{\alpha_3} \, (L_2 + L_1)^{\alpha_4} \, (L_2 - L_1)^{\alpha_5} \, (2L_3 - 1)^{\alpha_6}. \tag{4.4a}$$

Then

$$E := \int_K f \, d\xi d\eta \; = \; (-1)^{\alpha_5} 2\sqrt{3} \, I(\alpha_1, \alpha_2, \alpha_5) I(\alpha_3, \alpha_1 + \alpha_2 + \alpha_4 + \alpha_5 + 1, \alpha_6) \tag{4.4b}$$

where

$$I(i, j, k) := \int_0^1 (1 - t)^i \, t^j \, (1 - 2t)^k \, dt. \tag{4.4c}$$

Proof. Using (4.4a,b), we have

$$E \; = \; 2\sqrt{3} \int_T L_1^{\alpha_1} \, L_2^{\alpha_2} \, L_3^{\alpha_3} \, (L_2 + L_1)^{\alpha_4} \, (L_2 - L_1)^{\alpha_5} \, (2L_3 - 1)^{\alpha_6} \, dL_1 dL_2 \tag{4.5a}$$

where $T = \{(L_1, L_2) \,|\, 0 \le L_1, \, 0 \le L_2, \, L_1 + L_2 \le 1\}$. Using the change of variables $L_1 = (1 - x)y, \;\; L_2 = xy$, which maps the unit square $R = (0, 1) \times (0, 1)$ onto T, we get

$$E = (-1)^{\alpha_5} 2\sqrt{3} \int_R (1 - x)^{\alpha_1} \, x^{\alpha_2} \, (1 - 2x)^{\alpha_5} \Big\} \Big\{ y^{\alpha_1 + \alpha_2 + \alpha_4 + \alpha_5 + 1} \, (1 - y)^{\alpha_3} \, (1 - 2y)^{\alpha_6} \Big\} \, dx dy, \tag{4.5b}$$

which evaluates to (4.4b,c). □

As an example, consider the evaluation of the first term in (4.2) with

$$\hat{\phi}_i^2 = L_1 L_2 L_3 (L_2 - L_1)^{i_1} (2L_3 - 1)^{i_2}, \quad \hat{\phi}_j^2 = L_1 L_2 L_3 (L_2 - L_1)^{j_1} (2L_3 - 1)^{j_2}. \tag{4.6a}$$

Transforming to barycentric coordinates, we have

$$\begin{aligned}\frac{\partial\hat{\phi}_i^2}{\partial\xi}\frac{\partial\hat{\phi}_j^2}{\partial\xi} &= \frac{1}{4}\left(\frac{\partial\hat{\phi}_i^2}{\partial L_2}-\frac{\partial\hat{\phi}_i^2}{\partial L_1}\right)\left(\frac{\partial\hat{\phi}_j^2}{\partial L_2}-\frac{\partial\hat{\phi}_j^2}{\partial L_1}\right)\\ &= \frac{1}{4}L_3^2(L_2-L_1)^{i_1+j_1+2}(2L_3-1)^{i_2+j_2} \;+\\ &\quad i_1j_1L_1^2L_2^2L_3^2(L_2-L_1)^{i_1+j_1-2}(2L_3-1)^{i_2+j_2} \;+\\ &\quad \frac{1}{2}(i_1+j_1)L_1L_2L_3^2(L_2-L_1)^{i_1+j_1}(2L_3-1)^{i_2+j_2}, \qquad (4.6b)\end{aligned}$$

which may be integrated using (4.4).

Each face shape function of degree $k \le p$ in $\mathbf{\Psi}_p^s$, $\mathbf{\Psi}_p^c$, or $\mathbf{\Psi}_p^n$ is an expression of the form (2.3e). In Table 3, we list the first three polynomials $\mathcal{F}_{r_1r_2}$ for the Szabó, Carnevali, and the new basis. The polynomials are expressed as functions of $x = L_2 - L_1$ and $y = 2L_3 - 1$. A *MAPLE* program to evaluate these functions for arbitrary values of p using the orthogonalization process of Figure 3 appears in an Appendix to this paper.

p	Szabó	Carnevali	New
3	1	1	1
4	x	$-\frac{1}{4}\left(2x+y-\frac{1}{3}\right)$	x
	y	$\frac{1}{4}\left(2x-y-\frac{1}{3}\right)$	$y+\frac{1}{3}$
5	$\frac{3}{2}x^2-\frac{1}{2}$	$\frac{1}{16}\left((2x+y)^2+2x+y-\frac{2}{7}\right)$	$x^2+\frac{1}{14}y-\frac{1}{14}$
	xy	$-\frac{1}{16}\left((2x+y)(2x-y)-\frac{1}{7}\right)$	$xy+\frac{3}{7}x$
	$\frac{3}{2}y^2-\frac{1}{2}$	$\frac{1}{16}\left((2x-y)^2-(2x-y)-\frac{2}{7}\right)$	$y^2+\frac{4}{7}y-\frac{1}{21}$

Table 3: Function $\mathcal{F}_{r_1r_2}(L_1,L_2,L_3)$ associated with the two-dimensional face shape functions (2.3e) for the Szabó, Carnevali, and new bases. Polynomials are expressed in terms of $x = L_2 - L_1$ and $y = 2L_3 - 1$.

In Figure 4a we show the condition numbers $\kappa(M_p^t)$, $t = s, c, n$, as functions of p with the stiffness matrix M_p^t corresponding to the Laplacian according to (3.2). Again, the stiffness matrices have been scaled to have unit diagonal elements. As anticipated, orthogonalizing the face shape functions has resulted in a dramatic decrease in the condition number. In the range $3 \le p \le 14$, the condition number is growing as

$$\kappa(M_p^n) \approx p(\ln p)^{1.8} + 16\ln p. \qquad (4.7a)$$

This growth is a consequence of the coupling between the edge and face shape functions. This coupling can be eliminated by modifying the edge shape functions to be orthogonal

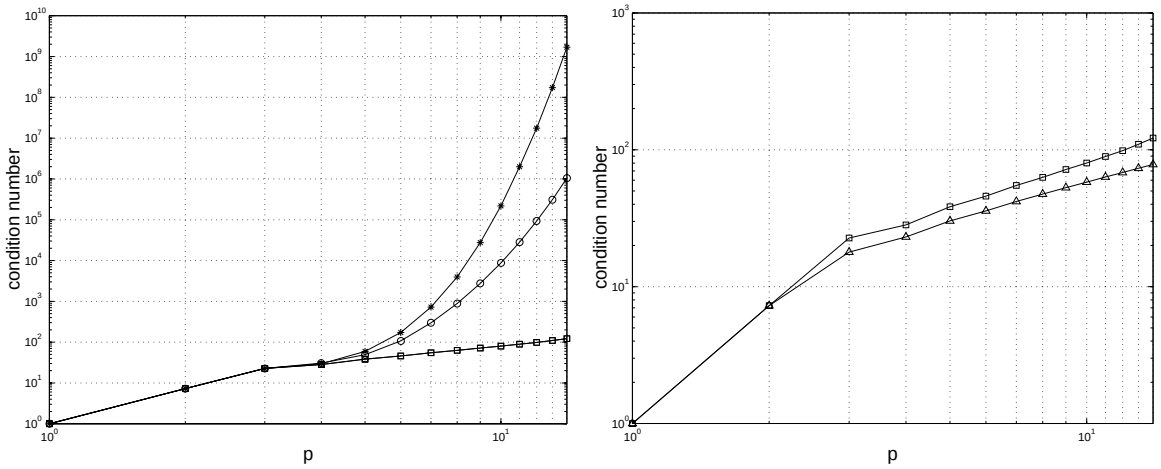

(a) (b)

Figure 4: (a) Condition numbers of M_p^s $(*)$, M_p^c $(\circ)$, and M_p^n $(\square)$ vs. p . (b) Condition number versus p for the local stiffness matrices M_p^n $(\square)$ and $\tilde{M}_p^n$ $(\triangle)$.

to the face shape functions. Letting $\tilde{\mathbf{\Psi}}_p^n$ be the resulting basis and $\tilde{M}_p^n$ the corresponding stiffness matrix, we compare $\kappa(\tilde{M}_p^n)$ and $\kappa(M_p^n)$, $p = 1, 2, \ldots, 14$, in Figure 4b. In the range $3 \le p \le 14$, we have

$$\kappa(\tilde{M}_p^n) \approx 5p + 3\ln p. \tag{4.7b}$$

Unfortunately, the basis $\tilde{\mathbf{\Psi}}_p^n$ is no longer hierarchical since the edge and face shape functions have to be orthogonal.

The sparsity, expressed as a percentage of the nonzero entries, of M_p^s, M_p^c, M_p^n, and $\tilde{M}_p^n$ is shown as a function of p in Figure 5. Sparsity increases steadily for M_p^c, M_p^n and $\tilde{M}_p^n$ as p increases and appears to settle at 65% for M_p^s. The stiffness matrix M_p^c is less dense than M_p^n as a result of (2.10) while $\tilde{M}_p^n$ is the most sparse with a density of approximately 9% when $p = 14$.

In order to appraise the conditioning of a global stiffness matrix with the choice of the basis, we consider the nonlinear reaction-diffusion problem

$$\frac{\partial u}{\partial t} - q(1-u)u^2 - \frac{1}{2}\Delta u = 0, \quad (x,y)^T \in \Omega := (0,1)\times(0,1), \;\; t > 0, \;\; q > 0, \tag{4.8a}$$

with initial and Dirichlet boundary conditions specified so that the exact solution is

$$u(x,y,t) = \frac{1}{1 + \exp\left(\sqrt{\frac{q}{2}}(x+y) - \frac{q}{2}t\right)}. \tag{4.8b}$$

This solution represents a wave-like front moving normal to the vector $(-1,1)$ with speed $\sqrt{q/2}$.

We solved (4.8a) with $q = 500$ on $0 < t \le 0.1$ using a uniform mesh of 32 triangles and a piecewise polynomial basis of (uniform) degrees $p = 1, 2, \ldots, 9$. Both the Szabó $\mathbf{\Psi}_p^s$

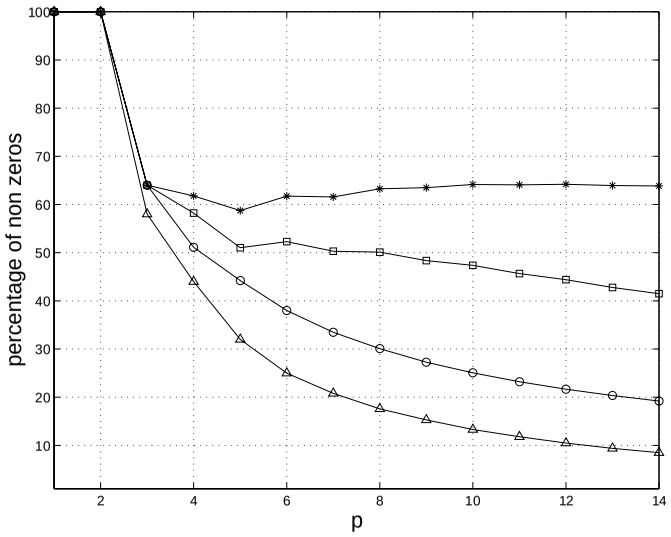

Figure 5: Percentage of non-zero entries of the local stiffness matrices M_p^s ($*$), M_p^c ($\circ$), M_p^n ($\square$) and $\tilde{M}_p^n$ ($\triangle$).

and the new $\mathbf{\Psi}_p^n$ bases were used. The condition numbers of the system Jacobian matrix at $t = 0.06$ are shown as functions of p and the number of degrees of freedom (DOF) in Figures 6a and b, respectively. They have been computed using the routine GECO from the LINPACK package. The growth of the condition number has, once again, been dramatically reduced with the new basis.

4.2 Three-Dimensional Shape Functions

In order to reduce the coupling between face and region shape functions and, consequently, the growth in the condition number of the stiffness matrix, we construct a hierarchical basis $\mathbf{\Psi}_p^n$ by (i) using the Szabó vertex and edge shape functions (2.6, 2.7), (ii) making the face shape functions orthogonal on each face, and (iii) making the region shape functions orthogonal. The orthogonal face shape functions are extracted from (2.8) and (4.3) using the Gram-Schmidt process (Figure 3). Region shape functions are obtained from (2.9) with

$$\mathcal{R}_{r_1 r_2 r_3}(t_1, t_2, t_3) = (t_2 - t_1)^{r_1}(2t_3 - 1)^{r_2}(2t_4 - 1)^{r_3} \tag{4.9}$$

using the Gram-Schmidt procedure.

Based on Lemma 2, we only need to construct the new face modes associated with one face (say face 1). The others can be obtained using obvious transformations.

Lemma 2. *Let $\phi(L_1, L_2, L_3)$ and $\psi(L_1, L_2, L_3)$ be smooth functions on the reference*

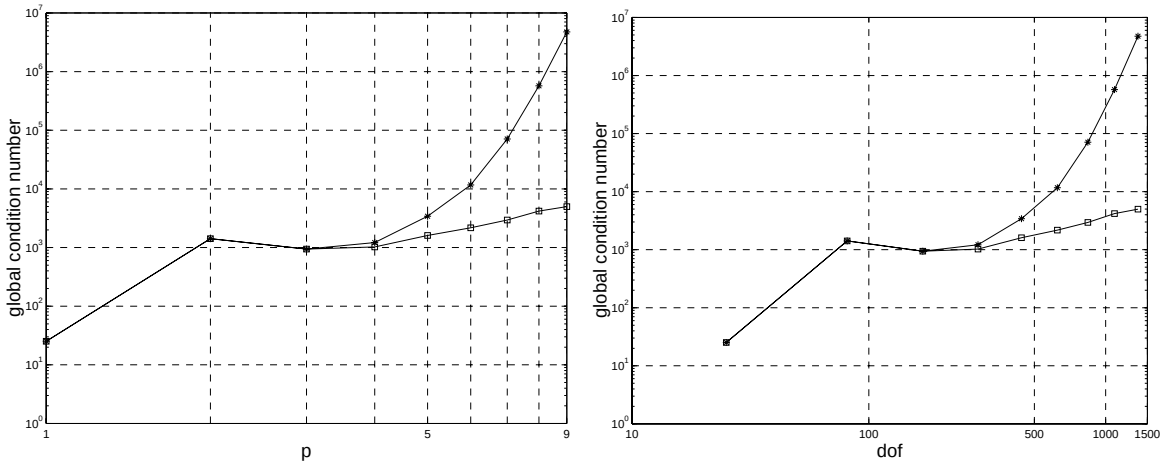

Figure 6: Condition number of the system Jacobian matrix of (4.8) versus p (a) and the degrees of freedom (DOF, b).

tetrahedron K and define

$$\phi_1(L_1,L_2,L_3) = \phi(L_2,L_3,L_4), \quad \psi_1(L_1,L_2,L_3) = \psi(L_2,L_3,L_4), \tag{4.10a}$$
$$\phi_2(L_1,L_2,L_3) = \phi(L_3,L_4,L_1), \quad \psi_2(L_1,L_2,L_3) = \psi(L_3,L_4,L_1), \tag{4.10b}$$
$$\phi_3(L_1,L_2,L_3) = \phi(L_4,L_1,L_2), \quad \psi_3(L_1,L_2,L_3) = \psi(L_4,L_1,L_2), \tag{4.10c}$$

with L_i, $i = 1,2,3,4$, given by (2.5). Then

$$\int_K \nabla\phi_i \cdot \nabla\psi_i \, d\xi d\eta d\zeta \;=\; \int_K \nabla\phi \cdot \nabla\psi \, d\xi d\eta d\zeta \tag{4.11}$$

with gradients computed relative to (ξ,η,ζ).

Proof. Using the chain rule

$$\frac{\partial}{\partial\xi} = \frac{1}{2}\left(\frac{\partial}{\partial L_2} - \frac{\partial}{\partial L_1}\right), \qquad \frac{\partial}{\partial\eta} = \frac{1}{2\sqrt{3}}\left(2\frac{\partial}{\partial L_3} - \frac{\partial}{\partial L_1} - \frac{\partial}{\partial L_2}\right),$$
$$\frac{\partial}{\partial\zeta} = \frac{1}{2\sqrt{6}}\left(3\frac{\partial}{\partial L_4} - \frac{\partial}{\partial L_1} - \frac{\partial}{\partial L_2} - \frac{\partial}{\partial L_3}\right) \tag{4.12}$$

with (4.10), we see that establishing (4.11) is equivalent to proving that

$$\int_{\hat{T}}\Big(6a_1(\phi_i)a_1(\psi_i) + 2a_2(\phi_i)a_2(\psi_i) + a_3(\phi_i)a_3(\psi_i)\Big)\, dL_1dL_2dL_3 \;=$$
$$\int_{\hat{T}}\Big(6a_1(\phi)a_1(\psi) + 2a_2(\phi)a_2(\psi) + a_3(\phi)a_3(\psi)\Big)\, dL_1dL_2dL_3, \tag{4.13a}$$

where

$$\hat{T} \;=\; \{(L_1,L_2,L_3)\,|\,0 \le L_1,\;\; 0 \le L_2,\;\; 0 \le L_3,\;\; L_1+L_2+L_3 \le 1\}\,, \tag{4.13b}$$

and

$$a_1(f) = \frac{\partial f}{\partial L_2} - \frac{\partial f}{\partial L_1}, \qquad a_2(f) = 2\frac{\partial f}{\partial L_3} - \frac{\partial f}{\partial L_1} - \frac{\partial f}{\partial L_2},$$
$$a_3(f) = 3\frac{\partial f}{\partial L_4} - \frac{\partial f}{\partial L_1} - \frac{\partial f}{\partial L_2} - \frac{\partial f}{\partial L_3}. \tag{4.13c}$$

We establish (4.13) with $i = 1$. Other cases proceed similarly. Thus, using (4.10a), we have

$$\begin{aligned} a_1(\phi_1) &= \frac{\partial \phi}{\partial L_1}(L_2, L_3, L_4) \\ a_2(\phi_1) &= 2\frac{\partial \phi}{\partial L_2}(L_2, L_3, L_4) - \frac{\partial \phi}{\partial L_1}(L_2, L_3, L_4) \\ a_3(\phi_1) &= 3\frac{\partial \phi}{\partial L_3}(L_2, L_3, L_4) - \frac{\partial \phi}{\partial L_1}(L_2, L_3, L_4) - \frac{\partial \phi}{\partial L_2}(L_2, L_3, L_4). \end{aligned} \tag{4.14a}$$

and

$$\begin{aligned} a_1(\psi_1) &= \frac{\partial \psi}{\partial L_1}(L_2, L_3, L_4) \\ a_2(\psi_1) &= 2\frac{\partial \psi}{\partial L_2}(L_2, L_3, L_4) - \frac{\partial \psi}{\partial L_1}(L_2, L_3, L_4) \\ a_3(\psi_1) &= 3\frac{\partial \psi}{\partial L_3}(L_2, L_3, L_4) - \frac{\partial \psi}{\partial L_1}(L_2, L_3, L_4) - \frac{\partial \psi}{\partial L_2}(L_2, L_3, L_4). \end{aligned} \tag{4.14b}$$

Substituting these into the left side of (4.13a) and introducing the change of variables $X = L_2$, $Y = L_3$, $Z = L_4$, which maps $\hat{T}$ onto itself, leads to

$$\int_{\hat{T}} \Big(6a_1(\phi_i)a_1(\psi_i) + 2a_2(\phi_i)a_2(\psi_i) + a_3(\phi_i)a_3(\psi_i) \Big)\, dL_1 dL_2 dL_3 =$$
$$\int_{\hat{T}} \Big(6a_1(\phi)a_1(\psi) + 2a_2(\phi)a_2(\psi) + a_3(\phi)a_3(\psi) \Big)\, dX dY dZ, \tag{4.15a}$$

which establishes the result. □

In Table 4, we list the first four polynomials $\mathcal{F}(x, y)$ and first three polynomials $\mathcal{B}(x, y, z)$ of the new basis on the reference tetrahedra. The face modes are listed for the face opposite to the vertex at $(0, 1/\sqrt{3}, 2\sqrt{2/3})$. Once again, the *MAPLE* program for evaluating these polynomials for arbitrary p appears in the Appendix.

We compute the condition numbers $\kappa(M_p^t)$, $t = s, c, n$, $p = 1, 2, \cdots, 10$, for local stiffness matrices M_p^t corresponding to the Laplacian operator (3.2) and present the results in Figure 7. The substantial improvement in the conditioning of M_p^n is clear. In the range $3 \le p \le 12$

$$\kappa(M_p^n) \approx p^2(\ln p)^3 + 20.9p(\ln p)^2. \tag{4.16}$$

The percentage of non-zero entries in M_p^s, M_p^c, and M_p^n as a function of p is shown in Figure 8. As in two dimensions, the percentage of nonzero entries in M_p^n decreases with p at about the same rate as M_p^s. The percentage of nonzero entries in M_p^c is significantly lower than both.

p	Face Modes
3	1
4	$x, \qquad y+\frac{3}{8}$
5	$x^2+\frac{89}{1425}y-\frac{709}{12825}, \qquad xy+\frac{59}{125}x, \qquad \frac{23382}{1364381}x^2+y^2+\frac{903388}{1364381}y-\frac{4165}{1364381}$
6	$x^3+\frac{1065}{6028}xy-\frac{681}{6028}x, \qquad x^2y+\frac{1495778}{2711133}x^2+\frac{16800371}{292802364}y^2-\frac{22840619}{1610413002}y-\frac{374750683}{16104130020}$ $\frac{11188}{992727}x^3+xy^2+\frac{3054670}{3639999}xy+\frac{335131}{3639999}x,$ $-\frac{4846821669}{208308582077}x^2y+y^3-\frac{3423671118}{208308582077}x^2+\frac{716173321035}{833234328308}y^2-\frac{10930991439}{416617164154}y-\frac{55006884029}{833234328308}$
	Region Modes
4	1
5	$x, \qquad y+\frac{1}{2}, \qquad \frac{1}{3}y+z+\frac{2}{3}$
6	$x^2+\frac{3}{50}y+\frac{3}{50}z+\frac{7}{825}, \qquad xy+\frac{14}{25}x, \qquad \frac{201}{14551}x^2+y^2+\frac{640847}{727550}y+\frac{603}{727550}z+\frac{1642}{14551},$ $\frac{173}{627}xy+xz+\frac{448}{627}x, \qquad -\frac{66816}{1636631}x^2+\frac{1635425}{4909893}y^2+yz+\frac{20883436}{24549465}y+\frac{4562522}{8183155}z+\frac{1831190}{4909893},$ $-\frac{15524}{902523}x^2+\frac{41641}{300841}y^2+\frac{654170}{902523}yz+z^2+\frac{475336}{902523}y+\frac{1159624}{902523}z+\frac{335332}{902523}$

Table 4: Functions $\mathcal{F}(x,y)$ and $\mathcal{B}(x,y,z)$ associated with the three-dimensional orthogonal face modes (2.8a) and region modes (2.9a) of degrees 3 through 6.

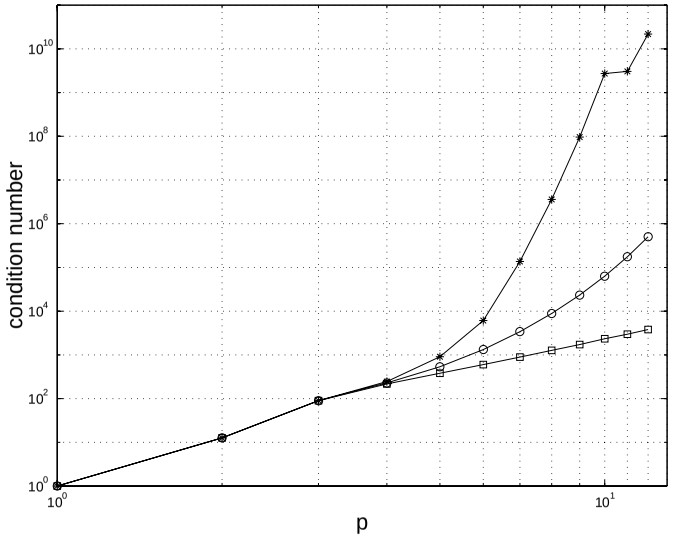

Figure 7: Condition numbers of M_p^s ($*$), M_p^c ($\circ$), and M_p^n ($\square$) vs. p

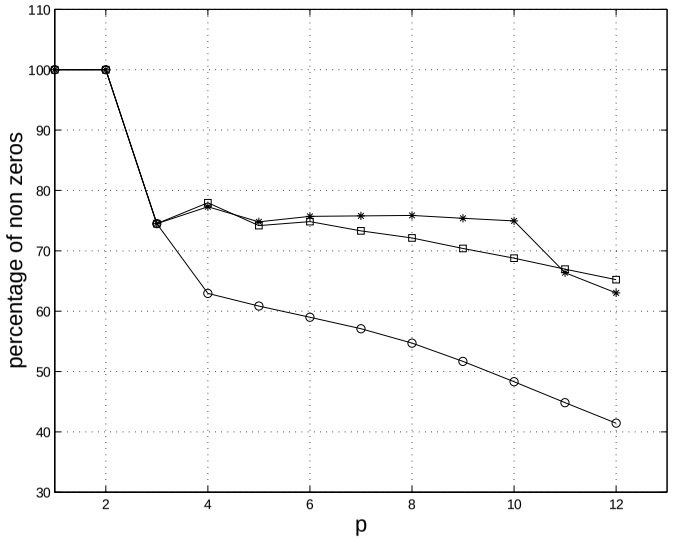

Figure 8: Percentage of non-zero entries of the local stiffness matrices M_p^s ($*$), M_p^c ($\circ$), and M_p^n ($\square$).

5 Discussion

We indicate how to construct hierarchical bases on triangles and tetrahedra that have a quadratic growth in the condition number with polynomial degree p. This is substantially better than the exponential growth associated with the hierarchical bases of Szabó and Babuška [10] and Carnevali *et al.* [3]. The new basis has reasonable sparsity which decreases as a percentage with increasing p. Stiffness matrices will, however, be less sparse than those of the Carnevali basis.

The strategy for improving the condition number involves extracting an orthogonal set of face shape functions in two dimensions and orthogonal face shape functions on each face and orthogonal region shape functions in three dimensions. The Gram-Schmidt procedure is relatively straight forward when the proper basis representations (4.3, 4.9) are used.

6 Appendix

We present a *MAPLE* implementation of the pseudocode algorithm shown in Figure 3. This software is available upon request.

The procedure `orth_modes()` generates the orthogonal face and region modes using the Gram-Schmidt process. The face modes on the reference triangle and tetrahedra and the region modes on the reference tetrahedra are constructed by orthogonalizing the elements of the set

$$\left\{ L_1 L_2 L_3 (L_2 - L_1)^{i_1} (2L_3 - 1)^{i_2} \mid \; i_1 + i_2 = 0, 1, \cdots \right\}, \tag{6.1}$$

and

$$\left\{ L_1 L_2 L_3 L_4 (L_2 - L_1)^{i_1} (2L_3 - 1)^{i_2} (2L_4 - 1)^{i_3} \mid \; i_1 + i_2 + i_3 = 0, 1, \cdots \right\}, \tag{6.2}$$

respectively. The resulting face and region modes are written as $L_1 L_2 L_3 \mathcal{F}(x, y)$ and $L_1 L_2 L_3 L_4 \mathcal{B}(x, y, z)$ respectively, where $x = L_2 - L_1$, $y = 2L_3 - 1$, $z = 2L_4 - 1$,

$$\mathcal{F}(x, y) = c_{1,1} + c_{2,1} x + c_{2,2} y + c_{3,1} x^2 + c_{3,2} xy + c_{3,3} y^2 + \cdots, \tag{6.3}$$

and

$$\begin{aligned} \mathcal{B}(x, y, z) = c_{1,1} &+ c_{2,1} x + c_{2,2} y + c_{2,3} z \\ &+ c_{3,1} x^2 + c_{3,2} xy + c_{3,3} y^2 + c_{3,4} xz + c_{3,5} yz + c_{3,6} z^2 + \cdots. \end{aligned} \tag{6.4}$$

The procedure `orth_modes()` uses a specialized integration procedure `E_PROD()` to evaluate integrals of the type (4.2).

```
orth_modes := proc(p,ent,d,flg)
# p   is the order of the basis.
# ent is 2 for face modes and 3 for region modes
# d   is 2 for triangular and 3 for tetrahedral basis
# flg if 1 the function F or G gets printed and
```

```
#     if 2 the coefficients c(i,j) get printed
local ps, nF, ix, k, i, j, m, B, c, beta, b, r, tp, F, x, y, z;
ps:=ent+1:
if p < ps  then  ERROR(`No Face Or Region Modes To Orthogonalize`);  fi:
nF:=binomial(p-1,ent):   # Number of internal modes
# Generate the exponents r, s, and t.
ix:=array(1..nF,1..3):    k:=1:
for i from ps to p do
  for j from 0 to i-ps do
    if ent=2 then
      ix[k,1]:=i-j-ps:    ix[k,2]:=j:    ix[k,3]:=0:    k:=k+1:
    else
      for m from 0 to i-j-ps do
        ix[k,1]:=i-j-m-ps:    ix[k,2]:=m:    ix[k,3]:=j:    k:=k+1:
      od:
    fi:
  od:
od:
# Compute the scalar products of the monomial face modes
B:=array(1..nF,1..nF):
for j from 1 to nF do
  for i from 1 to j do
    B[j,i]:=E_PROD(ix[i,1],ix[i,2],ix[i,3],ix[j,1],ix[j,2],ix[j,3],ent,d):
    B[i,j]:=B[j,i]:
  od;
od;
# Orthogonalize
beta:=array(1..nF):   c:=array(1..nF,1..nF):   b:=array(1..nF):
beta[1]:=1:   c[1,1]:=beta[1]:   b[1]:=B[1,1]:
for k from 2 to nF do
  for r from 1 to k-1 do
    tp:=0:
    for j from 1 to r do   tp:=tp+c[r,j]*B[k,j]:   od:
    beta[r]:=simplify( -tp/b[r] ):
  od:
  c[k,k]:=1:
  for j from 1 to k-1 do
    c[k,j]:=0:
    for r from j to k-1 do   c[k,j]:=c[k,j]+beta[r]*c[r,j]:   od:
  od:
  b[k]:=0:
  for j from 1 to k do
    tp:=0:
    for i from 1 to k do   tp:=tp+c[k,i]*B[i,j]:   od:
    b[k]:=b[k]+c[k,j]*tp:
  od:
od:
# Output the orthogonal face modes to the file out_modes
if flg=1 then
  F:=array(1..nF):
  for j from 1 to nF do
    F[j]:=x^ix[j,1]*y^ix[j,2]*z^ix[j,3]:
    for i from 1 to j-1 do
      F[j]:=F[j]+c[j,i]*x^ix[i,1]*y^ix[i,2]*z^ix[i,3]:
```

```
    od:
  od:
fi:
appendto(‘out_modes‘);   k:=0:
for i from ps to p do
  lprint(‘=================== p =‘,i);
  for j from 1 to  binomial(i-2,ent-1)  do
    k:=k+1:
    if flg=1 then
      lprint(k,F[k]);
    elif flg=2 then
      for m from 1 to k do   lprint(‘c[‘,k,‘,‘,m,‘] =‘,c[k,m],‘:‘);   od:
    fi:
  od:
  lprint(‘ ‘);
od:
writeto(terminal);
end:

E_PROD := proc(i1, i2, i3, j1, j2, j3, ent, d)
local L, bl, phi, psi, a, b, i, f, q, r, s, t, u, v;
L:= array(1..4):
#The blending function
bl:= L[1]*L[2]*L[3]:   if ent=3 then   bl:= bl*L[4]:   fi:
#The functions and their partial derivatives
phi:=bl*(L[2]-L[1])^i1*(2*L[3]-1)^i2*(2*L[4]-1)^i3:
psi:=bl*(L[2]-L[1])^j1*(2*L[3]-1)^j2*(2*L[4]-1)^j3:
a:= array(1..4):   b:= array(1..4):
for i from 1 to 4 do   a[i]:=diff(phi,L[i]):   b[i]:=diff(psi,L[i]):   od:
f:= (d*a[1]-a[2]-a[3]-a[4])*b[1]+(d*a[2]-a[3]-a[4]-a[1])*b[2]:
f:=f+(d*a[3]-a[4]-a[1]-a[2])*b[3]+(d*a[4]-a[1]-a[2]-a[3])*b[4]:
q:= convert( expand(f) , list );   v:= 0:
for i from 1 to nops(q) do
  r:=degree(q[i],L[1]):   s:=degree(q[i],L[2]):
  t:=degree(q[i],L[3]):   u:=degree(q[i],L[4]):
  v:=v+lcoeff(q[i])*r!*s!*t!*u!/(r+s+t+u+d)!:
od:
RETURN(v/(5-d));
end:
```

References

[1] I. Babuška, M. Griebel and J. Pitkäranta, *The Problem of Selecting the Shape Functions for a p-Type Finite Element,* Int. J. Num. Meth. Engng, Vol. 28, (1989), pp.1891-1908.

[2] I. Babuška and M. Suri, *The p- and h-p Versions of the Finite Element Method. An Overview,* Comp. Meth. in Appl. Mech. and Engng., 80 (1990) pp.5-26.

[3] P. Carnevali, R. B. Morris, Y. Tsuji and G. Taylor, *New Basis Functions and Computational Procedures for p-Version Finite Element Analysis,* Int. J. Num. Meth. Engng, 36, (1993), pp.3759-3779.

[4] P. G. Ciarlet, P. A. Raviart, *Interpolation Theory Over Curved Elements, with Applications to Finite Element Methods,* Comp. Meth. in Appl. Mech. and Engng, 1 (1972), pp.217-249.

[5] H. Kardestuncer and D. H. Noorie, *Finite Element Handbook,* McGraw-Hill, New York, 1987.

[6] M. Lenoir, *Optimal Isoparametric Finite Elements and Error Estimates for Domains Involving Curved Boundaries,* SIAM J. Numer. Anal., 3 (1986), pp.562-580.

[7] J. Mandel, *Two-Level Domain Decomposition Preconditioning for the p-Version Finite Elemenmt Method in Three Dimensions*, Int. J. Numer. Meths. Engng., 29 (1990) 1095-1108.

[8] J. Mandel, *Hierarchical Preconditioning and Partial Orthogonalization for the p-Version Finite Element Method*, Chapter 7 in T.F. Chan, R. Glowinski, J. Periaux, and O.B. Widlund, Eds., *Third. Int. Symp. on Domain Decomposition Methods for Partial Differential Equations*, SIAM, Philadelphi, 1990, 141-156

[9] M. R. Spiegel, *Mathematical Handbook of Formulas and Tables,* McGraw-Hill, New York, 1999.

[10] B. Szabó and I. Babuška, *Introduction to Finite Element Analysis,* John Wiley and Sons, New York, 1989.